Supplementary material: Impact of wind farm wakes on flow structures in and around downstream wind farms

Anja Stieren & Richard J. A. M. Stevens

May 29, 2022

The supplementary material for the manuscript *Impact of wind farm wakes on flow structures in and around downstream wind farms* includes an additional analysis on the velocity and momentum flux profiles throughout the wind farms in section 1. The following sections give an overview of the effects of the grid resolution (section 2), the domain size (section 3), and the simulation time (section 4). In section 5 the color plots of the manuscript are shown in a color-blind friendly version.

1 Development of the velocity and momentum flux profiles throughout the wind farms

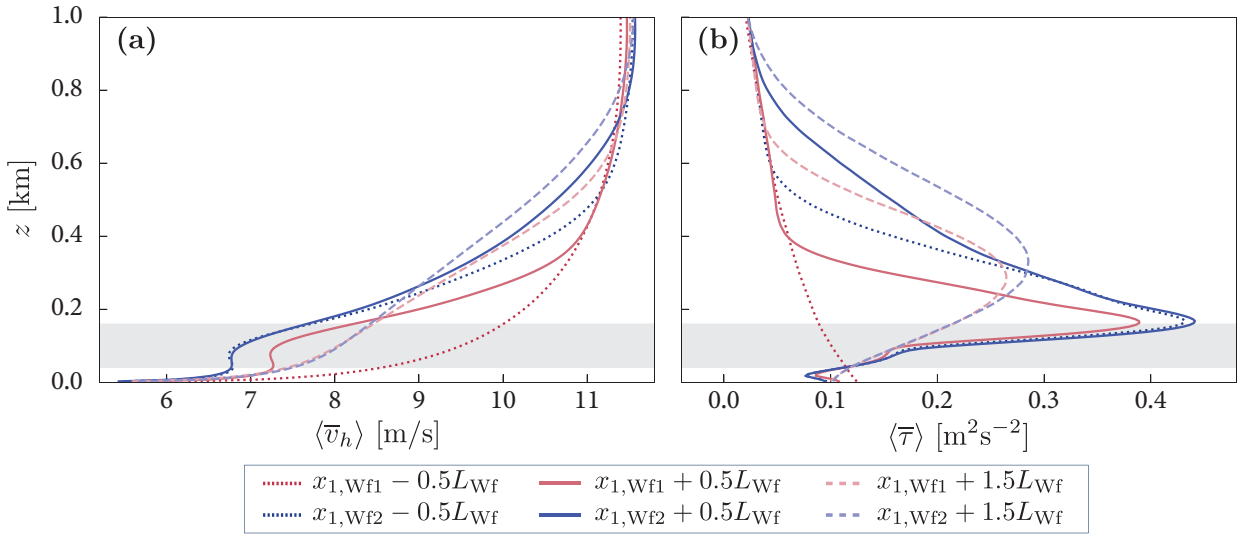

Figure 1: (a) Velocity and (b) momentum flux profiles at various positions in and around the upstream (Wf1) and downstream wind farm (Wf2) averaged over time and the spanwise extent of the wind farm for case stag-5km.

Figure 10 and figure 12 (a,b) in the manuscript show the time-averaged horizontal wind speed (averaged over the wind farm width) to compare the flow in and around the upstream and downstream wind farm. For a more quantitative comparison, figure 1 shows the spanwise averages of the velocity and momentum flux over the width of the wind farm at locations in front ($x_{1,\mathrm{Wf}} - 0.5L_{\mathrm{Wf}}$), in the center ($x_{1,\mathrm{Wf}} + 0.5L_{\mathrm{Wf}}$) and behind ($x_{1,\mathrm{Wf}} + 1.5L_{\mathrm{Wf}}$) each wind farm. Note, that the velocity at $0.5L_{\mathrm{Wf}}$ in front of the downstream wind farm (figure 1(a)) is lower than for the upstream farm at hub height and above the wind farm. The same holds for the velocity deficit in the center of the wind farms (at $0.5L_{\mathrm{Wf}}$). Behind the wind farm, differences between upstream and downstream farm are mostly visible above the turbines. Similar to the velocity profile, the largest differences in momentum flux (figure 1(b)) between upstream and downstream farm are observed above the turbines. The momentum flux is generally higher in and above the downstream farm.

2 Effect of grid resolution

To show that our main findings are not sensitive to the employed grid resolution, we performed two simulations for case stag-10km from the manuscript, one with a resolution of $\Delta x = 30$ m, $\Delta x = 15$ m, $\Delta z = 5$ m (original resolution in the manuscript) and a second simulation using a coarser resolution $\Delta x = 40$ m, $\Delta x = 20$ m, $\Delta z = 10$ m, see figure 2. For the latter, a smaller domain size is used to save computational resources. In the smaller domain, the first row of the upstream wind farm starts at 5 km instead of 7 km, and the last row is closer to the fringe region. In section 3.1 we further confirm that this does not affect the results. Figure 2 shows that there are only small differences between the simulations performed on different resolutions, showing that the results are not sensitive to the grid resolution.

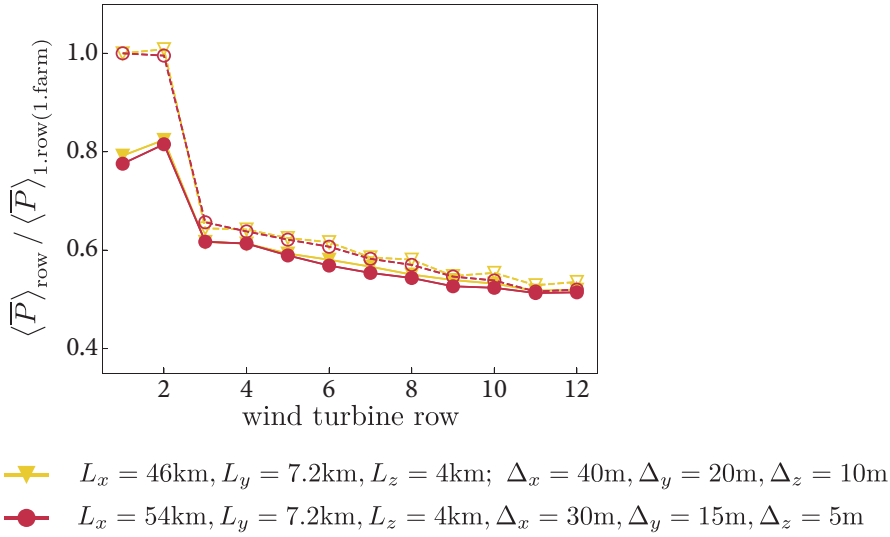

Figure 2: Comparison of simulations performed using different grid resolutions, the standard resolution used in the manuscript: $\Delta_x = 30$ m, $\Delta_y = 15$ m, $\Delta_z = 5$ m and a coarser mesh: $\Delta_x = 40$ m, $\Delta_y = 20$ m, $\Delta_z = 10$ m. Shown is the power production per row normalized by the performance of the first row of the upstream farm. Empty symbols: upstream farm; filled symbols: downstream farm.

3 Effect of domain size

In the following test cases, the resolution is coarser ($\Delta_x = 40$ m, $\Delta_y = 20$ m, $\Delta_z = 10$ m) than the resolution used in the manuscript ($\Delta_x = 30$ m, $\Delta_y = 15$ m, $\Delta_z = 5$ m) to reduce the computational costs. In section 2 we showed this does not affect the results. For the same reason, a shorter domain ($L_x = 46$ km) is considered and the first wind turbine row is positioned at $x = 5$ km, instead of $x = 7$ km (manuscript). The wind farm layout is staggered and the distance in between the farms is 10 km (case stag-10km). In section 3.1 and 3.2 we study the effect of the domain length and width, respectively.

3.1 Effect of domain length

Figure 3 compares the velocity profile averaged over the spanwise extent of the wind farms for two cases: a) a domain length of 46 km and b) a domain length of 57.5 km. As a result the last row is placed at either a) 10 km in front of the fringe region (comparable to case stag-15km) or b) 15.5 km in front of the fringe region (comparable to case stag-10km). The black line indicates the position 4 km in front of the fringe region in the shorter domain. Up to that position, there are only minor differences between the two cases. In the manuscript, all plots end at least 4 km in front of the fringe region. This test confirms that presented results in the manuscript are not affected by the used domain length.

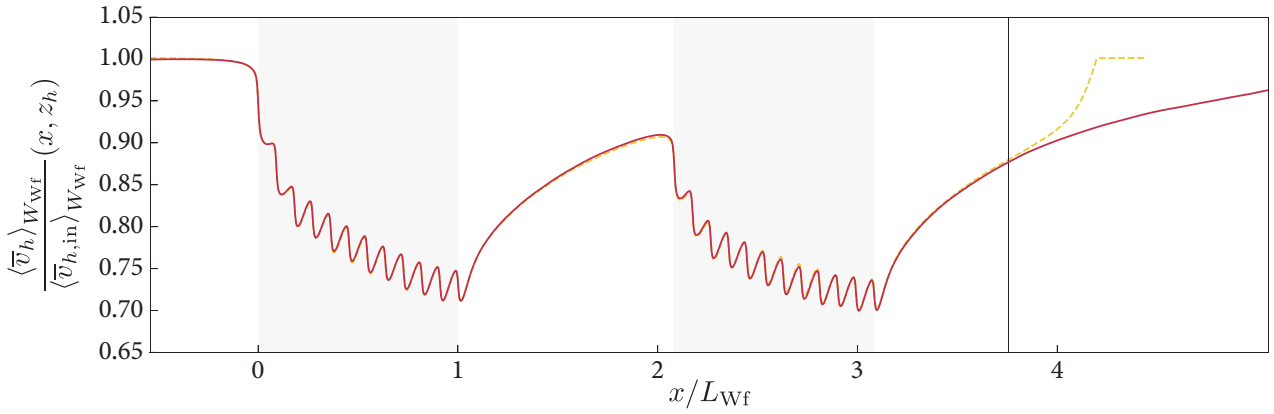

Figure 3: Horizontal velocity magnitude at hub height normalized by its inflow value averaged over the spanwise extent of the wind farm. The shaded regions indicate the streamwise location of each farm. Comparison of simulations for case stag-10km performed using different domain lengths, using the coarser $\Delta_x = 40$ m, $\Delta_y = 20$ m, $\Delta_z = 10$ m mesh. Distances to fringe region a) 10 km (comparable to case stag-15km); b) 15.5 km (comparable to case stag-10km). The black line indicates the position 4 km in front of the fringe region in the shorter domain. All plots in the manuscript end at least at this position.

3.2 Effect of domain width

To test the effect of the domain width, two cases are considered: a) $L_y = 7.2$ km and b) $L_y = 14.4$ km. Figure 4, which is comparable to figure 14 from the manuscript, shows only minor variations in the inflow conditions for each wind farm.

Figure 5 shows that the time-averaged horizontal velocity magnitude at hub height is comparable in both domains. However, high and low velocity streaks that are typical for neutral conditions [1] are visible in both domains.

Figure 6 shows the difference in the velocity profile between the two cases and figure 7 shows the difference in power production. The power production in the wider domain is lower than in the smaller domain as there is less blockage. We quantified the difference in total power production between the small and large domain to be 1.5% (i.e. $\frac{\langle P \rangle_{\mathrm{Wf1,wide}}}{\langle P \rangle_{\mathrm{Wf1narrow}}} = 0.985$ and $\frac{\langle P \rangle_{\mathrm{Wf2,wide}}}{\langle P \rangle_{\mathrm{Wf2,narrow}}} = 0.986$).

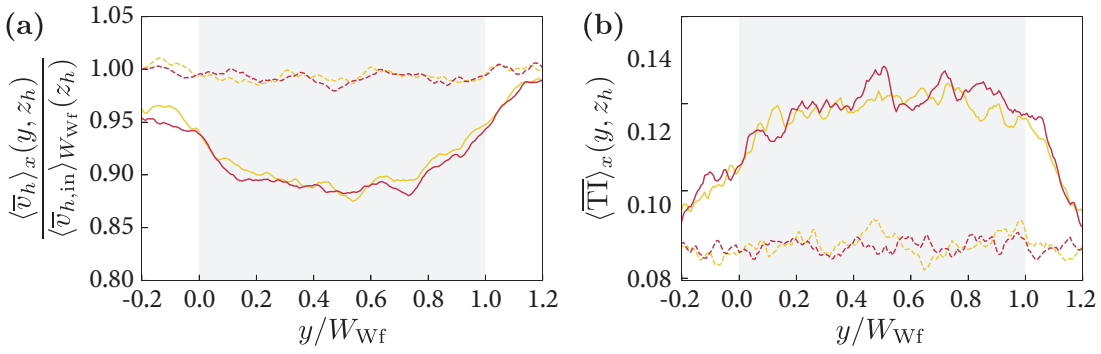

Figure 4: Comparison of simulations for case stag-10km performed on domains with different width, using the coarser $\Delta_x = 40$ m, $\Delta_y = 20$ m, $\Delta_z = 10$ m mesh. The domain width is varied from $L_y = 7.2$ km to $L_y = 14.4$ km. (a) Horizontal inflow velocity and (b) turbulence intensity at hub height. The average is taken from $x = 10D$ to $2D$ in front of each wind farm. The shaded area represent the wind farm position. Dashed lines: upstream farm; solid lines: downstream farm.

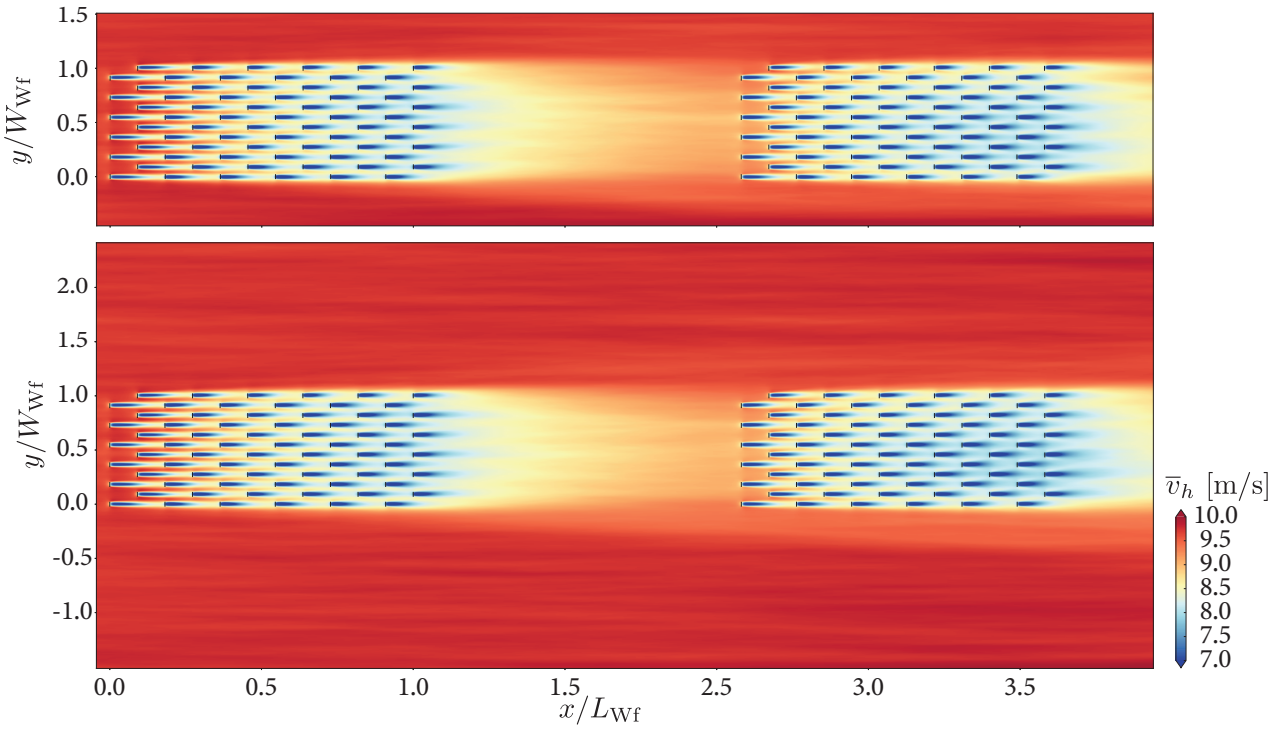

Figure 5: Comparison of simulations for case stag-10km performed on domains with different width, using the coarser $\Delta_x = 40$ m, $\Delta_y = 20$ m, $\Delta_z = 10$ m mesh. The domain width is varied from $L_y = 7.2$ km to $L_y = 14.4$ km. Time-averaged horizontal velocity magnitude at hub height.

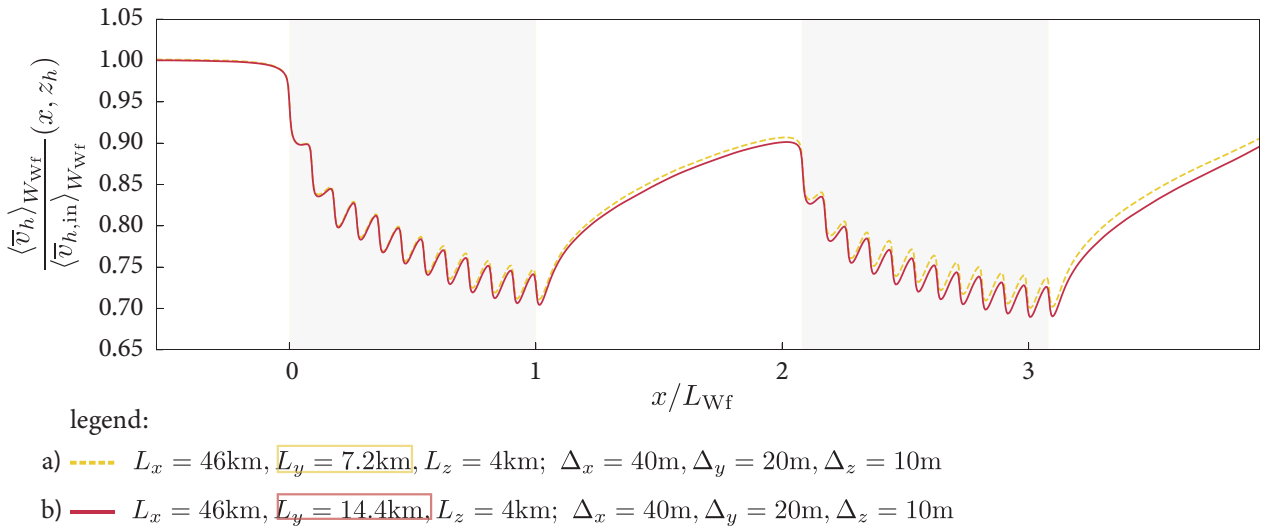

Figure 6: Comparison of simulations for case stag-10km performed on domains with different width, using the coarser $\Delta_x = 40$ m, $\Delta_y = 20$ m, $\Delta_z = 10$ m mesh. The domain width is varied from $L_y = 7.2$ km to $L_y = 14.4$ km. Horizontal velocity magnitude at hub height normalized by its inflow value averaged over the spanwise extent of the wind farm. The shaded regions indicate the streamwise location of each farm.

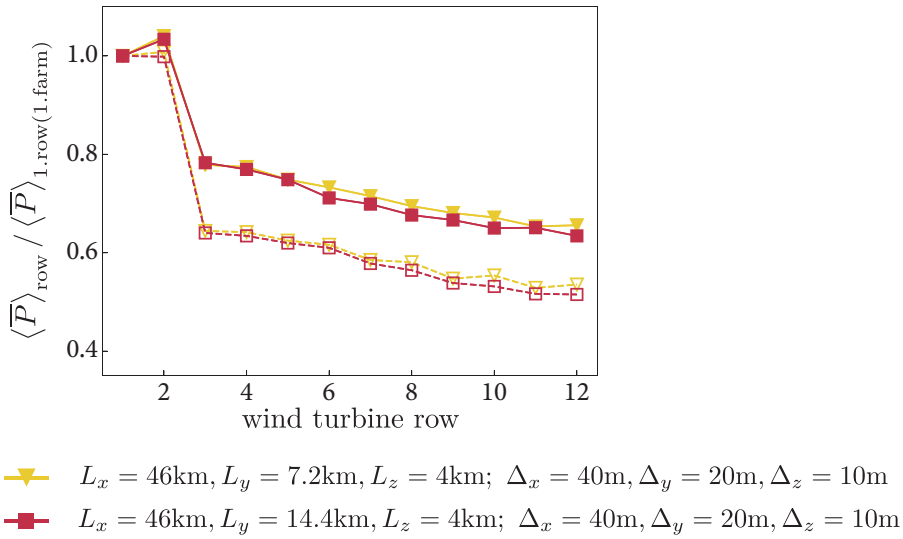

Figure 7: Comparison of simulations for case stag-10km performed on domains with different width, using the coarser $\Delta_x = 40$ m, $\Delta_y = 20$ m, $\Delta_z = 10$ m mesh. The domain width is varied from $L_y = 7.2$ km to $L_y = 14.4$ km. Power production per row normalized by the first row of the farm itself. Empty symbols: upstream farm; filled symbols: downstream farm.

4 Convergence of time averaged statistics

To test the convergence of the time averaged statistics we performed two simulations (on the same coarse grid as the test cases performed above) once time averaged over 5 hours and once over 10 hours. The simulations considered in the main manuscript are performed for 5 hours. Figure 8 shows that the averaged velocity profiles become smoother after additional averaging. However, the main findings remain unchanged, which is further confirmed in figure 9.

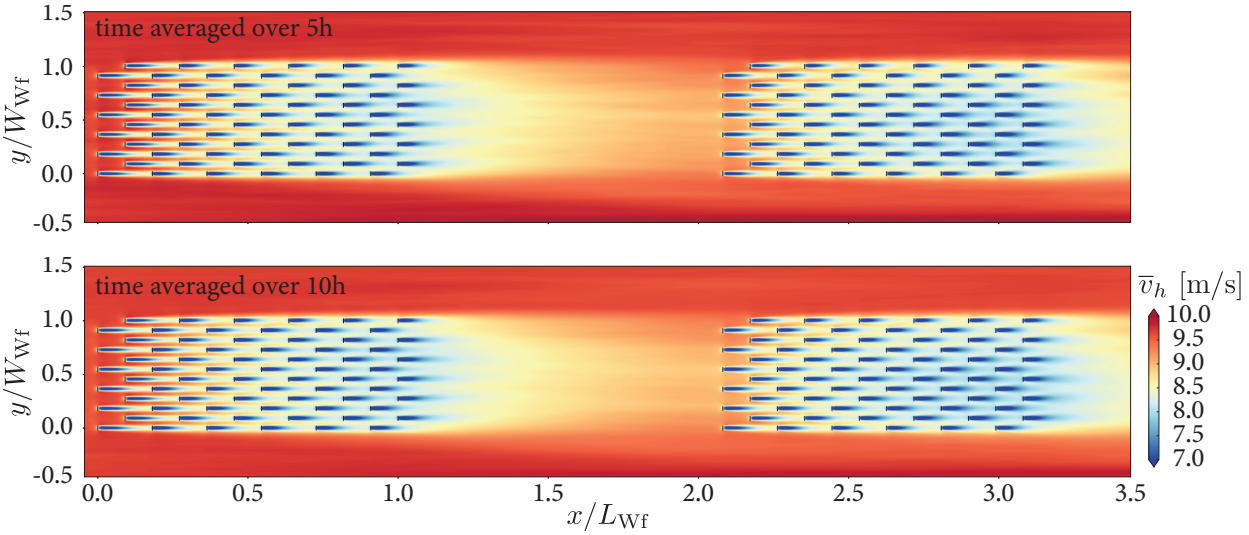

Figure 8: Visualization of the case stag-10km averaged over 5 hours and 10 hours.

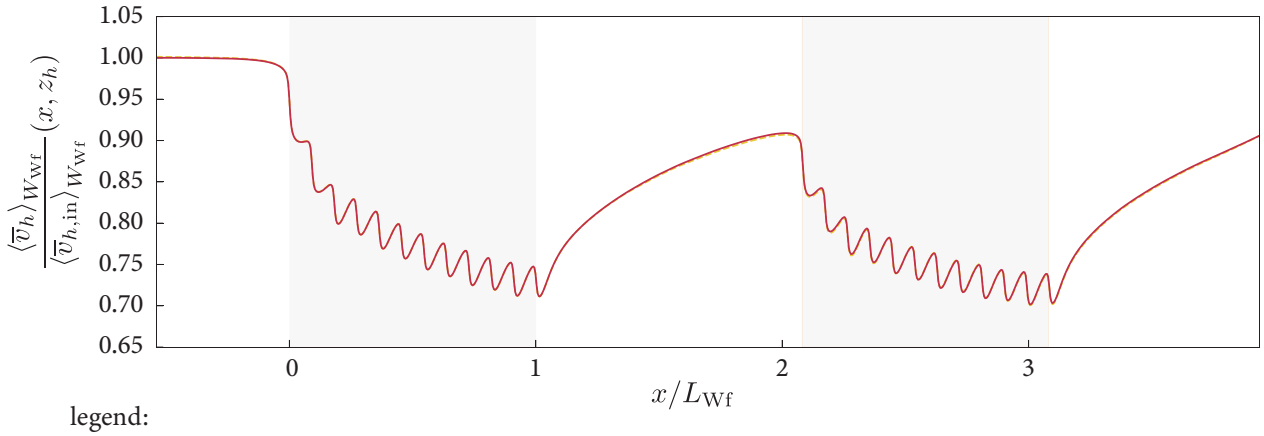

Figure 9: Comparison of case stag-10km time-averaged over 5 hours and 10 hours. Horizontal velocity magnitude at hub height normalized by its inflow value averaged over the spanwise extent of the wind farm. The shaded regions indicate the streamwise location of each farm.

5 Colorblind-friendly version of color-plots

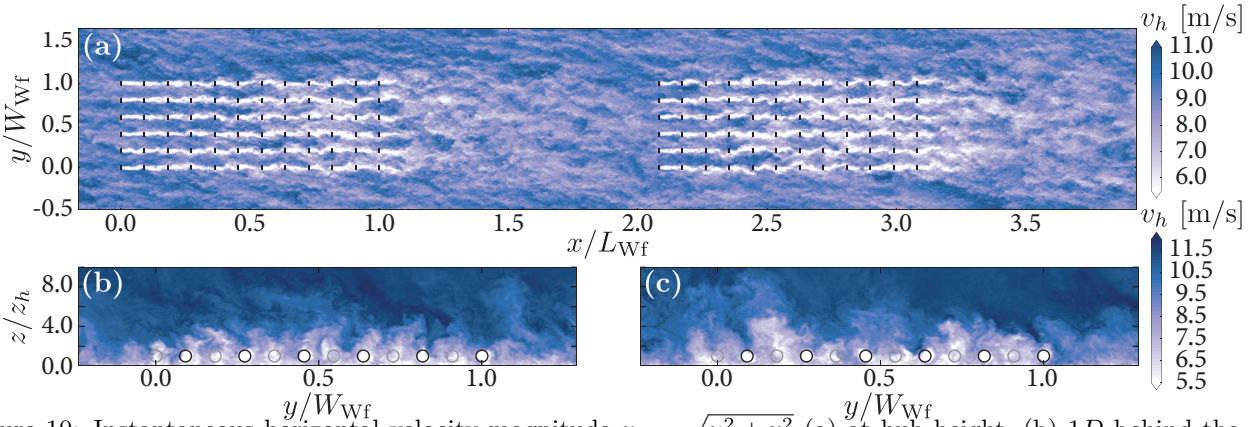

Figure 10: Instantaneous horizontal velocity magnitude $v_h = \sqrt{u^2 + v^2}$ (a) at hub height, (b) $1D$ behind the last row of the upstream wind farm and (c) $1D$ behind the last row of the downstream farm. The positions of the wind turbines are marked by (a) black lines and (b-c) circles. Circles indicate the spanwise-vertical location of the turbines for uneven (grey) and even (black) turbine rows.

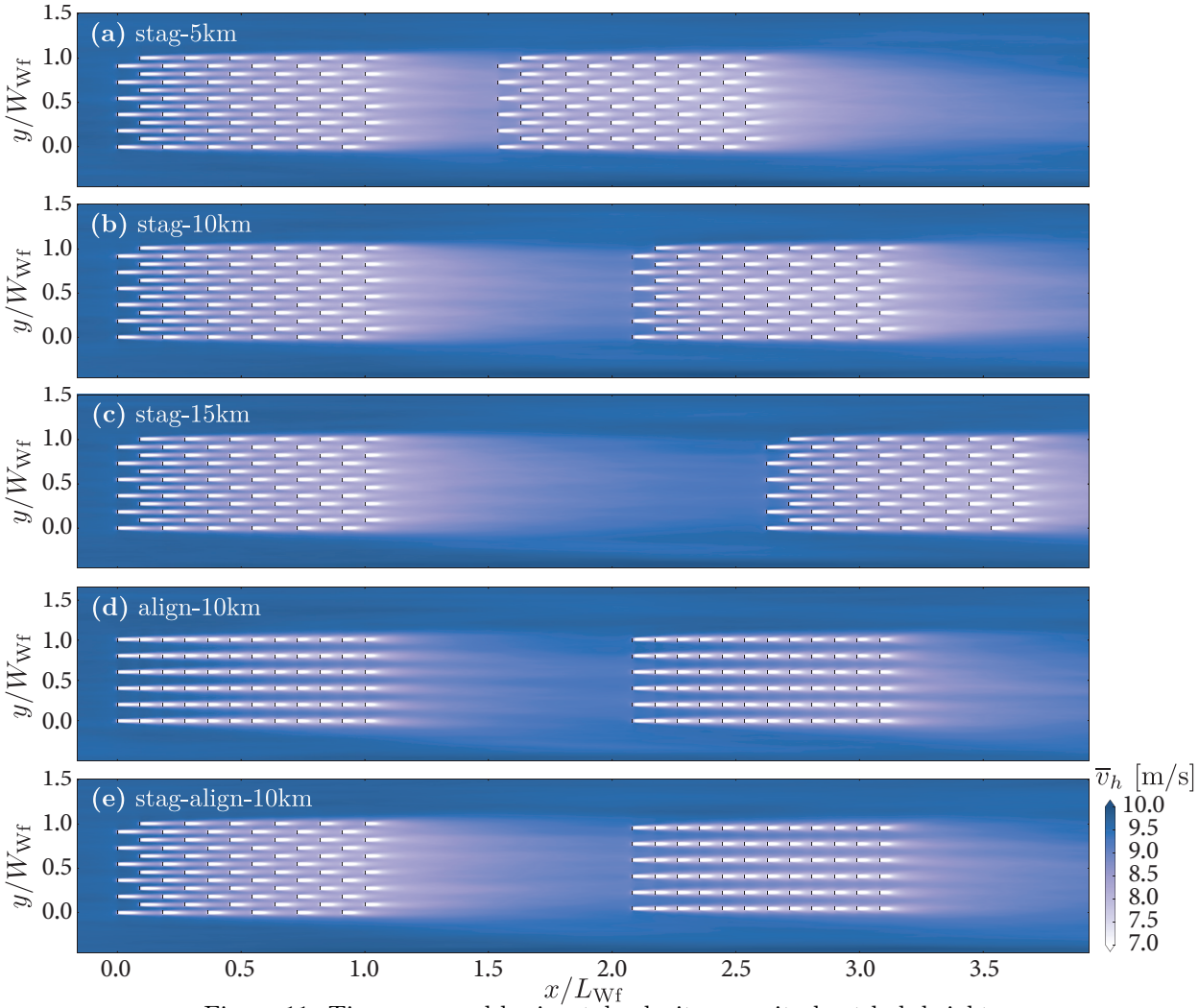

Figure 11: Time-averaged horizontal velocity magnitude at hub height.

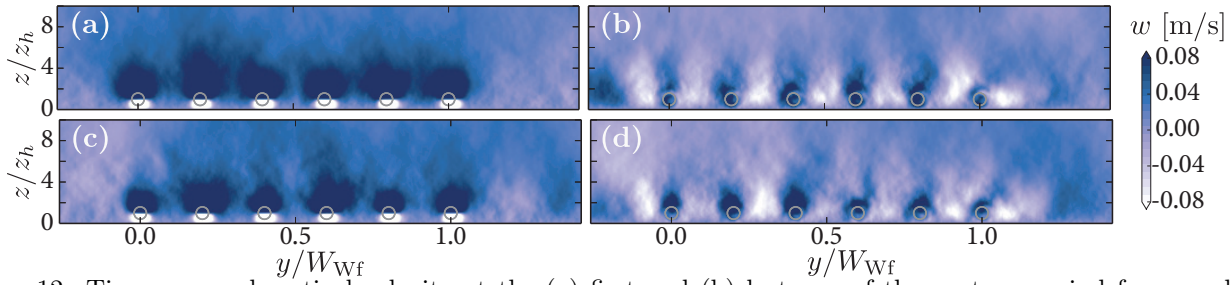

Figure 12: Time-averaged vertical velocity at the (a) first and (b) last row of the upstream wind farm, and the (c) first and (d) last row of the downstream wind farm for case align-10km. Grey circles denote the wind turbine positions.

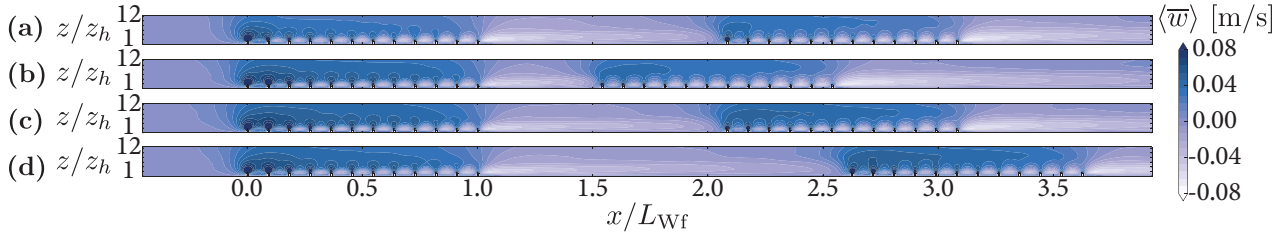

Figure 13: The vertical velocity, averaged over time and the spanwise wind farm extent for cases (a) align-10km, (b) stag-5km, (c) stag-10km, and (d) stag-15km. The aspect ratio is multiplied by a factor of 2 to increase the visibility.

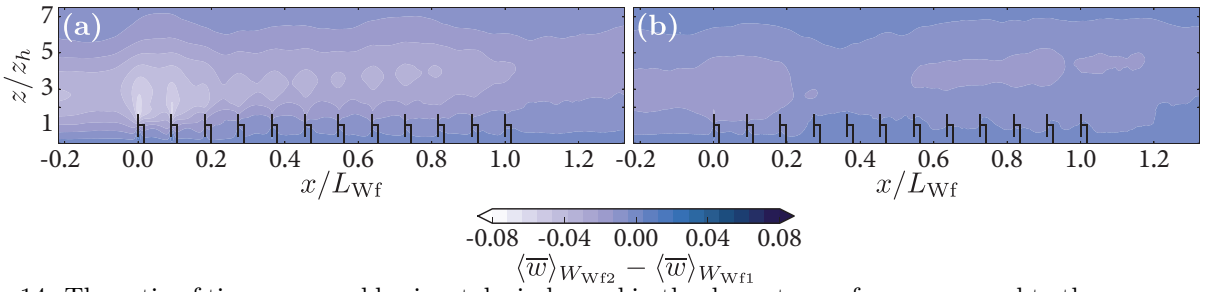

Figure 14: The ratio of time-averaged horizontal wind speed in the downstream farm compared to the corresponding upstream farm averaged over the wind farm width W_{Wf} for case (a) stag-5km and (b) stag-15km.

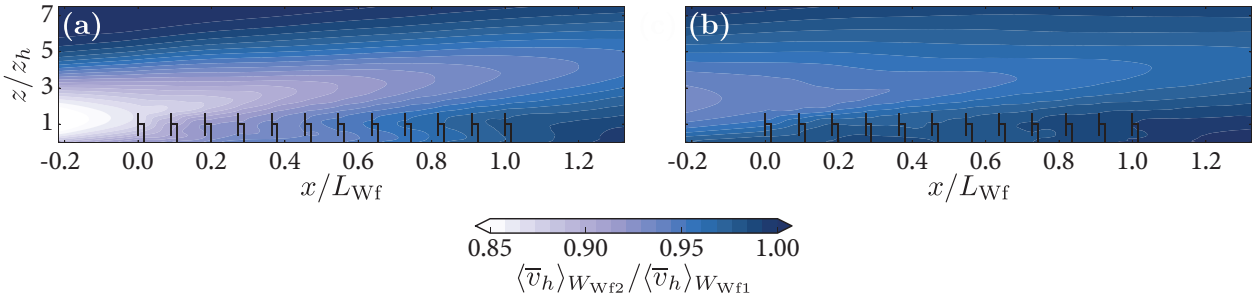

Figure 15: The differences between the time-averaged vertical velocity in the downstream and upstream farm averaged over the wind farm width W_{Wf} for case (a) stag-5km and (b) stag-15km.

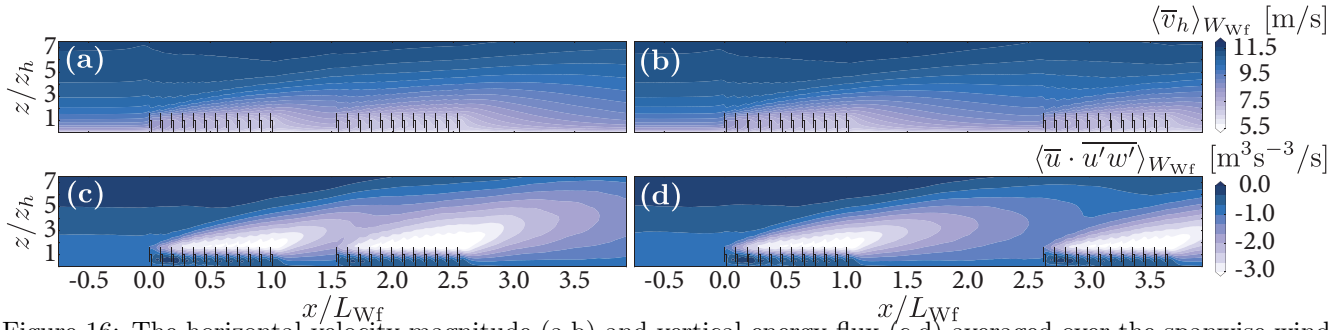

Figure 16: The horizontal velocity magnitude (a,b) and vertical energy flux (c,d) averaged over the spanwise wind farm extent for cases stag-5km (a,c) and stag-15km (b,d).

References

[1] Munters, W., Meneveau, C., and Meyers, J. (2016). Shifted periodic boundary conditions for simulations of wall-bounded turbulent flows. *Phys. Fluids*, 28:025112. doi:10.1063/1.4941912.